Lasers in Manufacturing Conference 2019

Cut Edge Structures and Gas Boundary Layer Characteristics in Laser Beam Fusion Cutting

Madlen Borkmann[a,b*], Achim Mahrle[b,a], Eckhard Beyer[a], Christoph Leyens[b, c]

[a]*TU Dresden, Institute of Manufacturing Science and Engineering, PO-Box, 01062 Dresden, Germany*
[b]*Fraunhofer-Institut für Werkstoff- und Strahltechnik IWS, Winterbergstraße 28, 01277 Dresden, Germany*
[c]*TU Dresden, Institute of Materials Science, PO-Box, 01062 Dresden, Germany*

Abstract

Fiber laser fusion cutting trials on AISI 304 stainless steel sheets of 10 mm thickness were performed to gain further insight into the formation mechanisms of topographical features of cut edges. It is found that particularly the variation of focus position causes distinct processing regimes with completely different cut edge structures. Standard cut edges can be divided in six different structural zones. It has become obvious that particular details of the different cut edge zones can be only understood as a result of a rather complex cutting gas flow. Corresponding high-resolution CFD simulations of the cutting gas elucidate the structure of the supersonic flow field and particular boundary layer characteristics. The results strongly support the hypothesis that the cutting gas flow and particularly the stability of the gas boundary layer plays an important role for the generation of the final cut edge topography.

Keywords: laser beam fusion cutting; cut edge structure; gas flow characteristics; gas boundary layer; modelling and simulation

1. Introduction

Laser beam fusion cutting is an established manufacturing process. It is based on a combined action of a laser beam to melt the material along the desired cut contour and a gas jet (nitrogen for fusion cutting, oxygen for reactive cutting with an inherent oxidation reaction) to blow the of the processing zone (Powell, 1998). A cut kerf is generated that separates the cut part from the surrounding raw material. Productivity

* Corresponding author. Tel.:+49 351 83391-3720; fax:+49 351 83391-3300.
E-mail address: madlen.borkmann@iws.fraunhofer.de.

and quality of the laser cuts are determined by the achievable cutting speed, the kerf geometry (size and shape), adherent dross as well as the topography of the resultant cut edge. The latter shows a characteristic striation structure that gives rise to specific roughness values.

The first attempts to describe and explain the resulting cut edge structures date back to the 1980's for the case of reactive CO_2 laser cutting. Schuocker, 1986 presumed that the striations are formed by an oscillating film of molten material. He considered different dynamic phenomena and related them to the striation wavelength and the formation of a double striation pattern. Vicanek & Simon, 1987 also linked the stability of the melt flow to the striation formation but for the case of fusion cutting. In their approach of a melt flow model they found different frequencies for the melt waves and for the resultant cut edge structure. They also analyzed fundamental features of the inert gas flow and distinguished different regimes with a dominant shear stress or a dominant pressure gradient effect. Schulz et al., 1999 developed a reduced model of the melt flow and analyzed the dynamic behavior of the system. A connection between the time-dependent front radius, striation formation and adherent dross was deduced. Detailed descriptions of resultant cut edge structures from experimental runs were already derived for CO_2 laser cutting. Schulz et al., 2009 distinguished different kind of ripples. They found ripples of the first kind in the upper part as a result of the moving melt front, ripples of second kind as result of the dynamic melt flow and ripples of the third kind formed by resolidified melt at the cut edges. However, solid-state laser cut edges usually show a much more irregular striation pattern and a lot of experimental and theoretical work was dedicated to explain those differences to CO_2 laser cutting. The state-of-the-art knowledge on this topic was recently summarized by Hirano, 2012. He also performed extensive experimental investigations and found periodical generations and downwards displacements of melt accumulations at the cut edges as the origin of striations. Also the stability of the central cut front melt flow was discussed as a primary factor for the final surface roughness. Other experimental studies were aimed at the visualization of the melt flow under processing-like conditions by trim-cut techniques. Yudin & Kovalev, 2007 found out by corresponding observations that the main part of the melt flows down at the kerf sides in strokes, rivulets and droplets in a certain distance to the cutting front. Ermolaev et al., 2014 revealed fundamental differences in the process characteristics between CO_2 and fiber laser cutting. A comprehensive overview of the development of the trim-cutting technique was recently given by Arntz et al. who also used the trim-cut technique to analyze the melt flow dynamics in cut kerfs (Arntz et al., 2017) and to demonstrate the possible impact of multiple reflections (Arntz et al., 2018).

These experimental investigations gave interesting insights into the dynamics of striation formation. However, underlying cause-effect relationships remain far from being fully understood. One interesting research topic is the role of the cutting gas flow and its impact on the final striation pattern on cut edges. Recent results on fiber laser cutting by Borkmann et al., 2018 revealed a close correlation between the measured roughness values and computed cut edge shear stress distributions. To prove direct relationships between striation pattern and gas flow characteristics, the current study gives additional insights into details of the cut edge topography and the flow characteristics of the cutting gas.

2. Experiments and characterization of cut edge topography

Cutting trials were performed on AISI 304 stainless steel sheets with a thickness of 10 mm using a 4 kW multi-mode fiber laser. Invariant laser and process parameters of a particular test series are summarized in Table 1. The focus position f_P as the primary factor in fiber laser cutting was varied between 0 mm at the top of the sheet to 10 mm at the bottom side with the aim to produce qualitatively different fiber laser cuts as shown in Figure 1. For all samples, the cutting speed corresponds to 80% of the achievable separation limit.

Table 1. Laser beam and process parameters

Parameter	Setting
Laser power	4 kW
M^2	10.3
Beam waist diameter	214 µm
Rayleigh length	3.3 mm
Nozzle type	conical, convergent
Nitrogen gas pressure	1.8 MPa
Nozzle stand-off	0.5 mm
Nozzle diameter	3.5 mm

It is obvious that the focus layer position has a decisive influence on the cutting performance and particularly on the cut edge structure. In fact, three principal categories can be distinguished by a pure visual inspection of the cut edges. Category 3 cuts (f_P = 10 mm) are produced for focus layer positions below the addressable optimal range and show pronounced melt accumulations in the upper part of the cut edge. The corresponding processing regime is usually avoided in practice because of the permanent risk of process interruptions. In contrast, category 2 cuts (f_P = 0, 2, 4 mm) are observable for a focus position above the addressable optimal range and can be characterized by more or less incomplete blow out of melt in the lower region of the kerf with extended burr formation. It is generally assumed that category 2 cuts are a result of a separation of the gas flow from the cut front caused by the overexpansion of the gas flow within the kerf and its discontinuous adjustment to the ambient pressure conditions (Zefferer et al., 1991). Category 1 cuts (f_P = 6, 8 mm) are cuts in the range of optimal focus layer positions and show edges with acceptable quality. The averaged roughness values (in the centerline of the sheet) are below R_a < 10 µm (R_z < 50 µm), there is only a minimum of remaining melt and no burr at the lower cut edge. Category 1 cuts show the characteristic cut edge structure of fiber laser fusion cutting with polymorphic striation forms and notable structural details. It is worthwhile to analyze those special features to get new insights into the mechanisms of striation formation.

The cut edge of category 1 cuts can be divided into characteristic zones. Figure 2 shows a high resolution image of a category 1 cut and additional detailed views of the defined zones. Primary striations forms as well as associated secondary features were evaluated. Zone 1a at the top of the kerf is characterized by small wavelength striations. In corresponding cross-sections of the kerf almost no resolidified melt is detectable and the striations are formed as valleys and ridges of the base material. Such a kind of striations was already reported by Schulz et al., 2009 as ripples of first kind. The striations in zone 1a are slightly curved in direction of the kerf front and are superimposed by wavy and dynamic flow patterns in the uppermost part. Below, the striations become almost vertical but still show a wavy structure. These vertical small wavelength striations continue in zone 1b but are here overlaid and partly covered by large-scale melt accumulations. These accumulations are backwards curved and cover several vertical striations. The structure resembles a droplet or rivulet flow pattern and the roughness in zone 1b is mainly determined by the accumulations. The multilayer structure in this zone implies the conclusion of a chronological order of the formation. It can be inferred that the vertical striations are formed in the vicinity of the front and are subsequently overlaid by a secondary rivulet melt flow. The next zone 2 is characterized by a sudden structural change. Vertical striations and melt rivulets abruptly terminate. Almost no striations or resolidified material can be detected in zone 2.

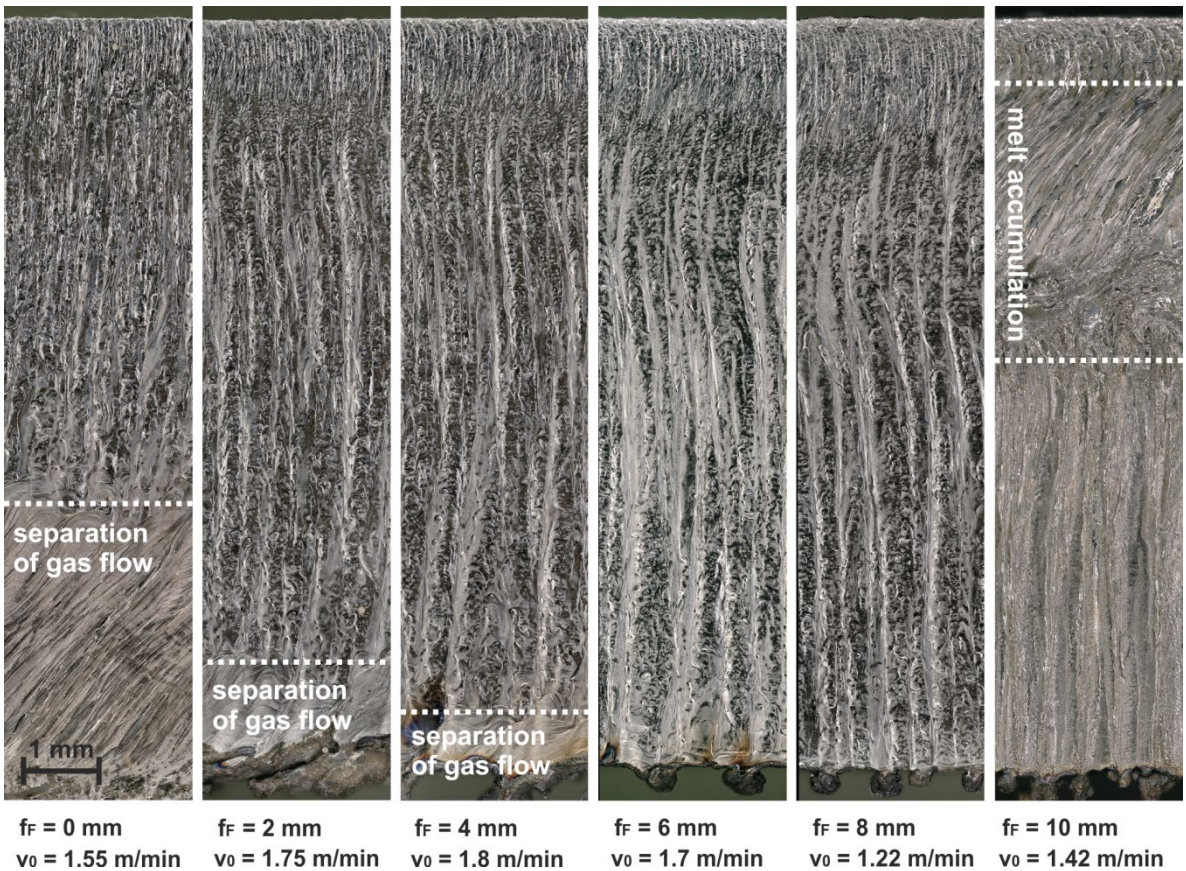

Fig. 1. Typical cut edge structures for variation of focus position. Focus position f_F=0-4 mm represent category 2, f_F=6-8 mm category 1 and f_F=10 mm category 3. Cutting direction from left to right.

Surprisingly, small cavities with diameters in the range of between 10 to 30 µm are prevalent features of this region. These cavities appear either alone or in groups and are uniformly distributed over the entire zone. Comparable cavity structures were already reported by Orishich et al., 2016 and Shulyatyev & Orishich, 2018 for reactive laser beam cutting with oxygen as a cutting gas. The origin of these cavities is however not conclusively resolved and the attempt to explain its occurrence as a result of the impact of droplets appears to be unlikely in the light of the almost round and regular shape and the absence of any droplet residuals. New striations with larger wavelength appear with the onset of zone 3. These striations are flat and seem to consist of only one layer of resolidified melt. In the area between the striations cavities and wavy structures are also present. In zone 4, the height of the striations is increased and they show a multilayer buildup. Lateral cross-sections of the ridges reveal one-sided profiles with a flat flank at the front side and a noticeably steeper flank at the back side. The area between the striations is filled with cavities and larger heaps of resolidified melt. These heaps are partly connected with path-like structures that are formed almost parallel to the primary striations. At the end of zone 4 some of the striations terminate and cause a slightly increase of the average striation wavelength. At the start of zone 5 the striations change their direction and get slightly backwards inclined. The one-sided profile with a steep and a flat flank is even pronounced but the overall height of melt buildup is comparable to zone 4.

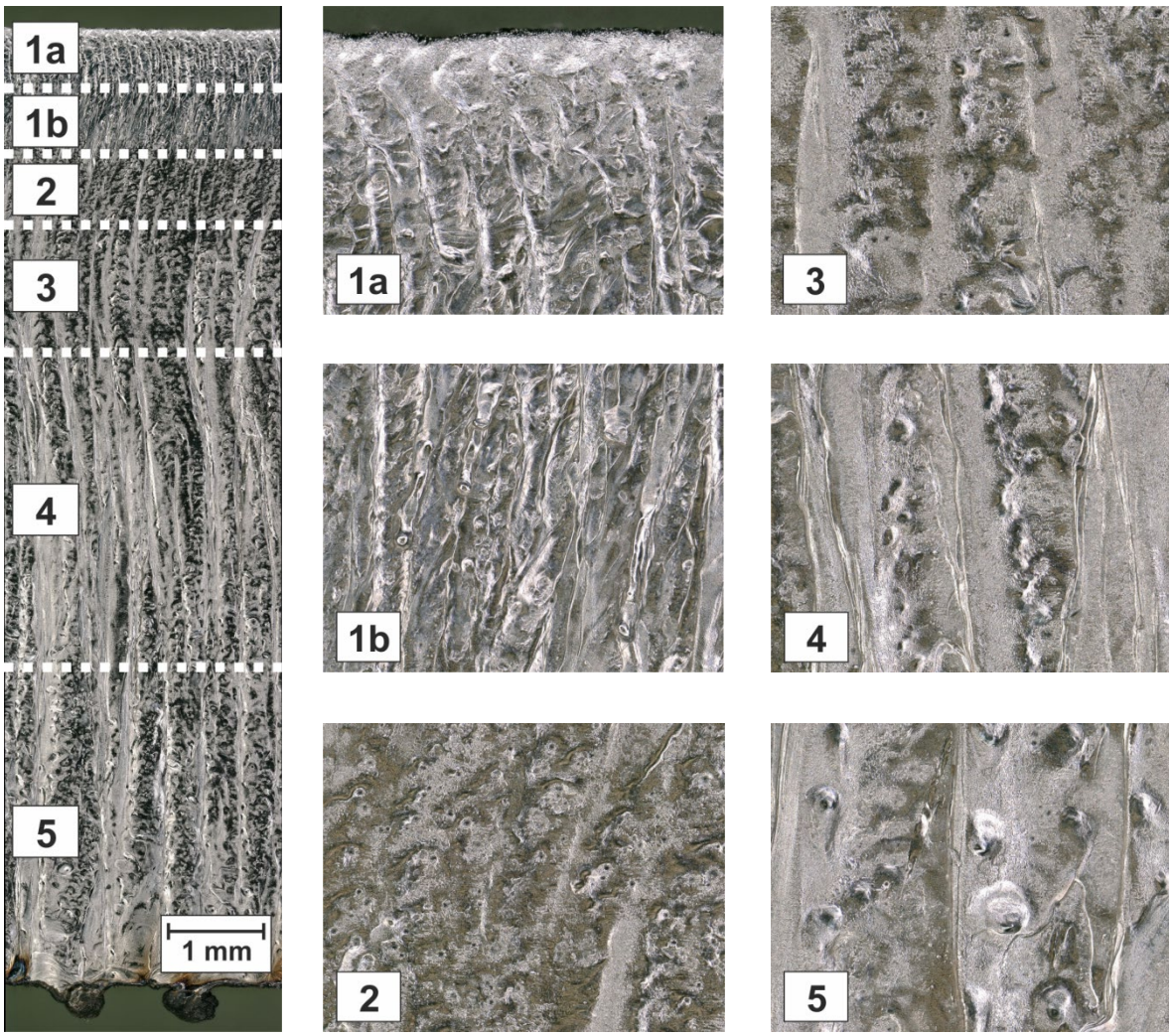

Fig. 2. Overview and partitioning of structural zones for a standard category 1 cut edge and detailed view for each zone. The detailed views are 750 µm in width. For structural description see text.

It is noteworthy that the heaps firstly emerged in zone 4 are developed to line-ups of larger melt accumulations at the flank of the ridges. The heaps are characterized by an obvious rotational structure like small shells, and all are oriented in the same rotational direction. It is therefore very likely that they are a footprint of a vortex or micro-sized “tornado” acting on the surface of the molten material.

It is concluded as a result of the detailed analysis of the cut edge structure that neither the shape of the polymorphic striations nor the characteristic secondary structures can be explained by currently available theories. In particular, the so far unreported secondary micro-structures support the view of a strong influence of the gas flow on the resulting cut edge structure. Available simulation models of the high-pressure and supersonic gas flow in narrow cut kerfs and corresponding experimental studies were able to reveal only main characteristics of the gas flow but do not address the structure of its boundary layer that transfers the momentum of the gas flow as shear forces onto the surface of molten material. The

topographic structure of the cut edges clearly indicates that an improved understanding of the striation formation process requires insights into details of the boundary layer development of the cutting gas flow.

3. Numerical investigations and characterization of flow structures of the cutting gas

The commonly applied high values of gas pressure in laser fusion cutting result in a supersonic gas flow with a complex and highly three-dimensional shock structure. Especially for small nozzle distances, the cut kerf acts as a kind of nozzle extension and the acceleration of the gas flow to supersonic velocities takes place within the kerf. The simulation of such flows can be performed by a solution of the Reynolds-Averaged Navier-Stokes equations (RANS equations) in combination with an appropriate turbulence model (k-ω SST). The computational domain is actually limited to a cut kerf in a 6 mm thick sheet to reduce the numerical efforts on the necessary high-resolution finite-volume mesh with local volume sizes down to 1 µm. The kerf itself is assumed to be parallel-sided with a width of 800 µm. The cut kerf front is approximated by a perpendicular half-cylinder. Furthermore an attached nozzle with 3 mm outlet diameter and a lengthwise symmetry plane were defined. It is supposed that the approach of an attached nozzle does not fundamentally alter the gas flow characteristics within the kerf especially in comparison to arrangements with small nozzle distances as commonly realized in laser beam fusion cuttings. Nitrogen was used as cutting gas as in the real experiments. Its thermodynamic state behaviour is described by the state equation of ideal gases in the addressed pressure range. Furthermore, the temperature dependence of the viscosity is modelled by the well-known Sutherland approach. The nozzle inlet boundary conditions was fixed to 1.5 MPa (15 bar) inlet pressure, whereas the outlet pressure boundaries were all set to ambient pressure conditions. No-slip conditions were applied for all wall boundaries with reasonable cut edge and cut front temperature distributions (T_{max} = 2500 K).

The resulting velocity distribution in the symmetry plane and the pressure distribution at the cut edge are shown in Figures 3 and 4. It is obvious that the applied high-resolution mesh in combination with high-order discretization methods is able to reproduce the complex shock structure of the gas flow very precisely. The shock structure determines the entire gas flow. The speed of sound is reached at the narrowest flow cross-section at the kerf entrance and a characteristic compression shock is formed along the upper kerf edge (Figure 3, region V1). This compression shock proceeds in flow direction and self-intersects in the symmetry-plane (region V3). The location of the shock can be detected in the velocity distribution in Figure 3 by a suddenly decelerated flow. A particularly intense deceleration can be also detected in the region where the side and front shocks intersect in a small area at approximately 0.75 mm depth (region V2). After the intersection, the shock is impinging on the opposite kerf edge. This impingement is related to a pressure rise in the corresponding boundary layer and causes the formation of a separation zone (Babinsky & Harvey, 2011). The pressure rise is clearly noticeable in the wall pressure distribution (Figure 4, region P1) at approximately 1 mm depth. In a shock-boundary-layer-interaction (SBLI) with separation, the impinging shock is reflected as two single shocks with reduced pressure rise, one at separation and one at reattachment. This pair of weaker shocks can be detected in the velocity distribution underneath the first shock intersection (Figure 3, region V4). In the next SBLI of the weaker shocks (region P2) the pressure rise at the wall is noticeably weaker. Furthermore, the pressure distribution at the wall is determined by the expansion, acceleration and a pressure decrease in the main stream of the gas flow.

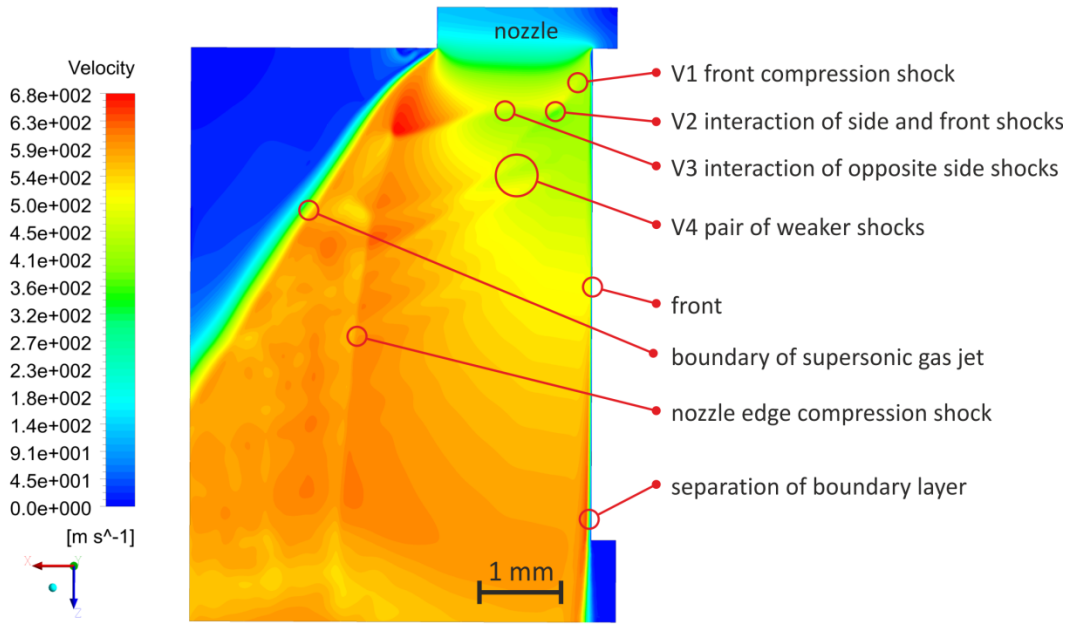

Fig. 3. Velocity distribution at symmetry plane. Simulation parameters: parallel-sided kerf with a width of 800 µm and a depth of 6 mm, 3 mm nozzle diameter, 1.5 MPa nitrogen gas pressure and a reasonable temperature distribution with a maximum of 2500 K at the front.

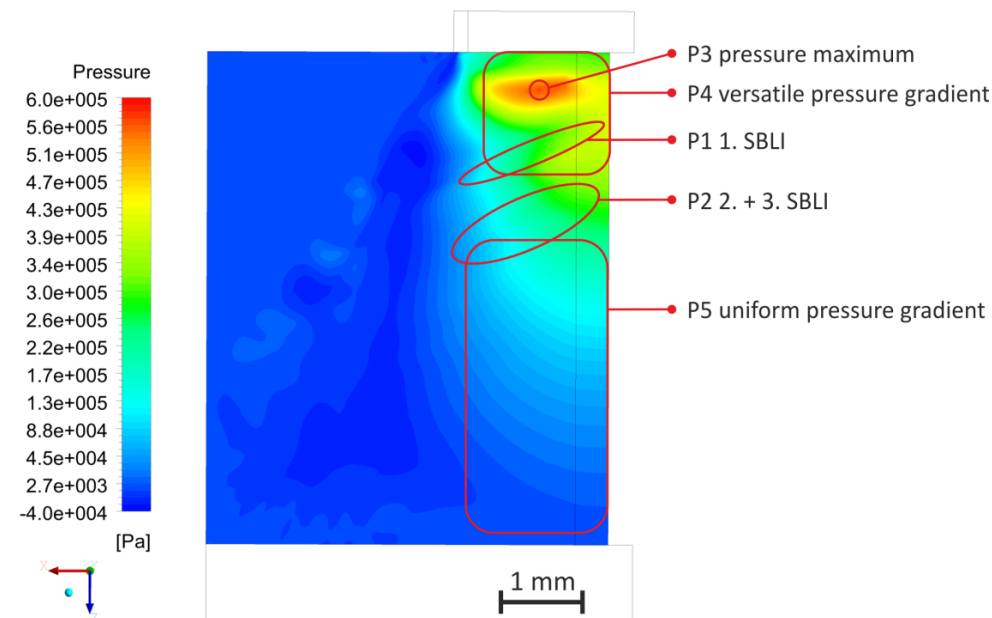

Fig. 4. Wall pressure distribution at cut edge and front. Simulation parameters: parallel-sided kerf with a width of 800 µm and a depth of 6 mm, 3 mm nozzle diameter, 1.5 MPa nitrogen gas pressure and a reasonable temperature distribution with a maximum of 2500 K at the front.

A global pressure maximum is formed at the side wall at approximately 0.5 mm depth (region P3). Consequently, a wall pressure gradient with strong local variations arises in a stripe of 1.5 mm depth (region P4). Afterwards a monotonic pressure decrease is found with a negative pressure gradient slightly inclined to the back of the kerf (region P5).

A visualization of the simulated vortex structure of the gas flow within the cut kerf is shown in Figure 5 by use of the so-called λ_2-criterion. It is obvious that the vortex distribution is rather complex. The area with the inflow of the gas into the kerf shows a recirculating separation zone associated with the compression shock. Within this separation zone a lateral modulation of the boundary layer and the formation of vertical vortices are induced. Following a first re-attachment, vertical vortices with small lateral wavelength are generated at the front and side. These vortices interact afterwards with the first SBLI. As a result, a separation and recirculation zone is formed and two weaker shocks are reflected. The second and third SBLI refer to this pair of shocks on the opposite kerf side and cause only a marginal separation without a recirculation. Consequently, a single reflection occurs that results in a fourth and fifth SBLI as shown in Figure 5. Subsequent to the first SBLI the decay and detachment of the small-wavelength vortices and the formation of new vortices with larger wavelength are observed. These new vortices are modulated in interaction with the further SBLIs but continue to exist beyond the global separation at the bottom edge of the kerf.

The irregular wall pressure gradient deduced from the wall pressure in Figure 4 determines the characteristics of the gas boundary layer, in particular its stability and the transition from a laminar into a turbulent state. Close to the upper edge of the kerf, the gas boundary layer can be assumed as laminar (Schlichting & Gersten, 1997). But for the cutting gas flow with a Reynolds number normally greater than 10^5 a transition of the boundary layer into the turbulent state will occur in a certain distance to the upper edge.

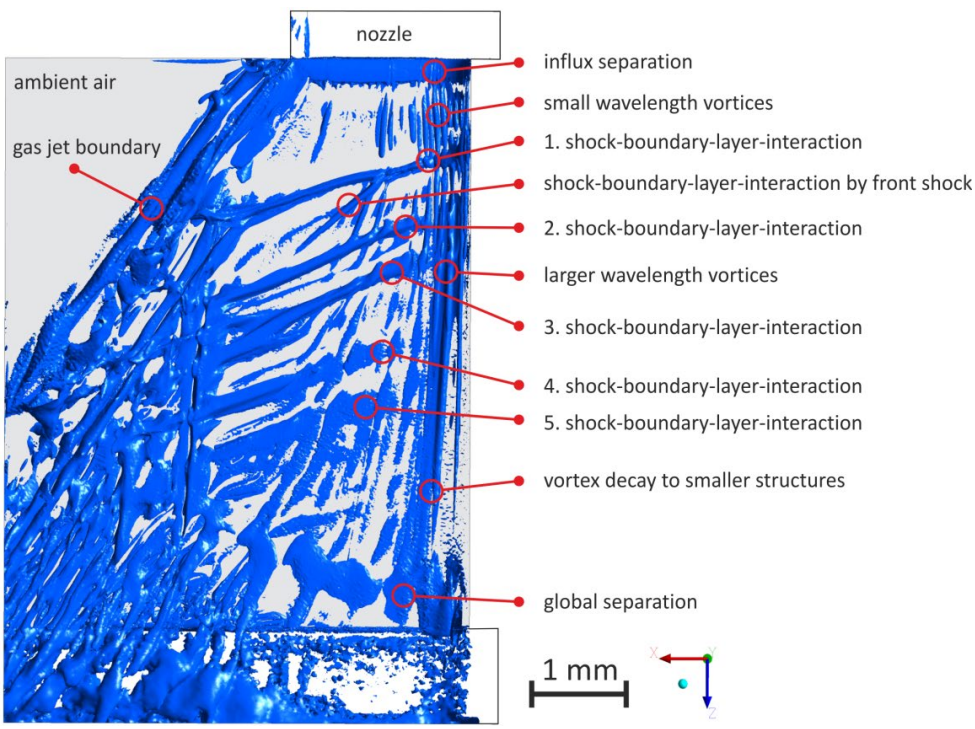

Fig. 5. Vortex visualization based on λ_2-criterion for the gas flow within a kerf of 800 µm width and 6 mm depth.

As shown in Figure 4 the pressure gradient possesses a significant component in lateral (or crosswise) direction. This crosswise pressure gradient at the wall results in a secondary crossflow within the boundary layer with a three-dimensional velocity distribution normal to the wall. This provokes a characteristic roll-up of the resulting shear layer – a phenomenon that is known as the so-called crossflow instability (Arnal et al., 1984, Reed & Saric, 1989 and Bippes & Nitschke-Kowsky, 1990). Those co-rotating crossflow vortices develop at the edge of the boundary layer and are nearly aligned with the main flow. The rotational direction of the vortices is determined by the crosswise pressure gradient and is altered by the first SBLI. Thus, the newly emerging large-wavelength vortices after the first SBLI at a depth of 1 mm have a changed rotational direction while the already existing counter rotating vortices are damped and decaying. Subsequently, the large-wavelength crossflow vortices are amplified and develop through different transition stages. Finally, the crossflow vortices break up into smaller vortices and induce the transition into a turbulent boundary layer regime.

Also a number of secondary instabilities of crossflow vortices are reported (Mielke, 1999, Janke & Balakumar, 2000, Wassermann et al., 2002, White & Saric, 2005 and Bonfigli & Kloker, 2007). The shape of those secondary instabilities shows certain conformity to the structures found at the lower cut edge by the microscopic characterization of the striation structure.

Furthermore it is suggested that the modulation of the boundary layer by crossflow vortices and SBLIs results in a modified shear stress distribution and also affects the heat fluxes at the kerf sides and the cutting front. It is highly reasonable to infer that the flow of the thin melt film is modulated likewise and that this modulation is imprinted on the cut edge within the solidification area.

4. Summary and Conclusions

Cutting trials on 10 mm AISI 304 stainless steel sheets using a 4 kW multi-mode fiber laser were analyzed by microscopy. Three different quality categories were defined which mainly depend on the position of the focus plane. For high quality cuts of category 1 a detailed investigation of the resulting cut edge structure was presented. As a result of detected features of striations and secondary structures, a partition into distinct structural zones could be introduced. Especially the shape of the secondary structures supports the view that the cutting gas flow and in particular the gas boundary layer strongly influence the cut edge topography.

Therefore high-resolution numerical simulations of the gas flow within the cut kerf were performed. The applied numerical methods are able to model the complex shock structure of the gas flow and its interaction with the gas boundary layer very precisely. The numerical simulation revealed a so far unreported vortex structure close to the cut front and edge. This vortex structure is attributable to the instability of the boundary layer and its interaction with the shock structure of the supersonic gas flow. Although basic relations were found, further investigations on the boundary layer instability are required for a deeper process understanding and improvement suggestions.

Based on the findings a qualitative correlation between the detected structural features of the cut edge and the complex flow structure of the cutting gas is derived for the first time as summarized in Table 2. It can be noted that a close relationship between the detected structural features of the cut edge and particular characteristics of the gas flow is confirmed. It is suggested that the modulation of the boundary layer by the primary crossflow vortices results in the formation of the striations whereas the cavities, heaps and wavy structures at the cut edge arise from the secondary instabilities of the vortices.

Table 2. Suggested correlations between gas flow characteristics and structural zones on kerf edges

Gas flow characteristics	Structural zone	Structural features
Influx separation and small wavelength vortices	1a	Small wavelength striations
Separation, recirculation and strong crosswise flow due to the first SBLI at the side interacting with small wavelength vortices	1b	Vertical small wavelength striations overlaid by melt rivulets
Detachment and decay of small wavelength vortices	2	Small cavities and almost no striations
Amplification of vortices with larger wavelength	3	New flat striations
Further amplification of vortices and initiation of secondary instabilities	4	Striations with multi-layer build-up and one-sided profile, onset of heaps
Saturation of primary CF-vortices and amplification of secondary structures	5	Striations with line-ups of heaps with co-rotational structure
Global separation with low shear	6	Melt accumulation

Acknowledgements

The authors appreciate the financial support given by the German Research Foundation (DFG) within the project “Evaluierung dynamischer Lösungsansätze zur Optimierung des Inertgasschneidens von Dickblech mit Laserstrahlquellen hoher Strahlqualität”, Contract No BE 1875/36-1.

References

Arnal, D., Habiballah, M. & Coustols, E. (1984). LAMINAR STABILITY THEORY AND TRANSITION CRITERIA IN TWO AND THREE-DIMENSIONAL FLOW. Recherche Aerospatiale (English Edition) (2).

Arntz, D., Petring, D., Jansen, U. & Poprawe, R. (2017). Advanced trim-cut technique to visualize melt flow dynamics inside laser cutting kerfs. Journal of Laser Applications, 29 (2), 22213.

Arntz, D., Petring, D., Stoyanov, S., Jansen, U., Schneider, F. & Poprawe, R. (2018). In situ visualization of multiple reflections on the cut flank during laser cutting with 1 µ m wavelength. Journal of Laser Applications, 30 (3), 32206.

Babinsky, H. & Harvey, J. K. (2011). Shock Wave Boundary Layer Interactions (Cambridge Aerospace Series). Cambridge: Cambridge University Press.

Bippes, H. & Nitschke-Kowsky, P. (1990). Experimental study of instability modes in a three-dimensional boundary layer. AIAA Journal, 28 (10), 1758-1763.

Bonfigli, G. & Kloker, M. (2007). Secondary instability of crossflow vortices. Validation of the stability theory by direct numerical simulation. Journal of Fluid Mechanics, 583, 229.

Borkmann, M., Mahrle, A. & Beyer, E. (2018). Study of correlation between edge roughness and gas flow characteristics in laser beam fusion cutting. Procedia CIRP, 74, 421-424.

Ermolaev, G. V., Yudin, P. V., Briand, F., Zaitsev, A. V. & Kovalev, O. B. (2014). Fundamental study of CO2- and fiber laser cutting of steel plates with high speed visualization technique. J. Laser Appl., 26 (4), 042004-1-9.

Hirano, K. (2012). Study on striation generation process during laser cutting of steel. Thèse, Arts et Métiers ParisTech - Centre de Paris. Paris.

Janke, E. & Balakumar, P. (2000). On the Secondary Instability of Three-Dimensional Boundary Layers. Theoretical and Computational Fluid Dynamics (14), 167-194.

Mielke, C. (1999). Numerische Untersuchungen zur Turbulenzentstehung in dreidimensionalen kompressiblen Grenzschichtstromungen (Fortschritt-Berichte VDI. Reihe 7, Stromungstechnik, Nr. 374). Dusseldorf: VDI Verlag.

Orishich, A. M., Shulyatyev, V. B. & Filon, A. E. (2016). Craterlike structures on the cut surface after oxygen-assisted laser cutting of steel. Journal of Laser Applications, 28 (1), 12007.

Powell, J. (1998). CO2 laser cutting (2nd ed.). Berlin: Springer.

Reed, H. L. & Saric, W. S. (1989). Stability of Three-Dimensional Boundary Layers. Annual Review of Fluid Mechanics (21), 235-284.

Schlichting, H. & Gersten, K. (1997). Grenzschicht-Theorie. Mit 22 Tabellen (9., völlig neubearb. und erw. Aufl.). Berlin: Springer.

Schulz, W., Kostrykin, V., Nießen, M., Michel, J., Petring, D., Kreutz, E. W. et al. (1999). Dynamics of ripple formation and melt flow in laser beam cutting. J.Phys.D: Appl. Phys., 32, 1219-1228.

Schulz, W., Nießen, M., Eppelt, U. & Kowalick, K. (2009). Simulation of Laser Cutting. In The Theory of Laser Materials Processing. Springer Series in Material Science (S. 21-69). Springer Netherlands.

Schuocker, D. (1986). Physical Mechanism And Modeling Of Laser Cutting. In S. Sottini & S. Trigari (Hrsg.), 1986 Int'l European Conf on Optics, Optical Systems, and Applications (SPIE Proceedings, S. 390). SPIE.

Shulyatyev, V. B. & Orishich, A. M. (2018). Microcraters and surface quality in laser oxygen cutting of thick steel sheets. Journal of Laser Applications, 30 (2), 22003.

Vicanek, M. & Simon, G. (1987). Hydrodynamical instability of melt flow in laser cutting. J.Phys.D: Appl. Phys., 20, 140-145.

Wassermann, P., Kloker, M. & Wagner, S. (2002). Secondary Instability of Steady and Unsteady Crossflow Waves. In S. Wagner, U. Rist, H.-J. Heinemann & R. Hilbig (Hrsg.), New Results in Numerical and Experimental Fluid Mechanics III. Contributions to the 12th STAB/DGLR Symposium Stuttgart, Germany 2000 (Notes on Numerical Fluid Mechanics (NNFM), Bd. 77, S. 247-254). Berlin, Heidelberg: Springer Berlin Heidelberg.

White, E. B. & Saric, W. S. (2005). Secondary instability of crossflow vortices. Journal of Fluid Mechanics, 525, 275-308.

Yudin, P. & Kovalev, O. (2007). Visualisation of events inside kerfs during laser cutting of fusible metal. Paper 1401. In 26th Int. Congress on Applications of Lasers & Electro-Optics (S. pp. 772–779).

Zefferer, H., Petring, D. & Beyer, E. (1991). Investigations of the gas flow in laser beam cutting. In Deutscher Verband für Schweißtechnik e.V. -DVS-, Düsseldorf: 3. Internationale Konferenz Stahltechnik ´91. Düsseldorf: DVS-Verlag, 1991 .